ACS APPLIED MATERIALS & INTERFACES

Research Article

www.acsami.org

Synthesis of Highly Branched Gold Nanodendrites with a Narrow Size Distribution and Tunable NIR and SERS Using a Multiamine Surfactant

Wenfeng Jia, Jinru Li, and Long Jiang*

Beijing National Laboratory for Molecular Science, Key Laboratory of Colloids and Surface, Institute of Chemistry, Chinese Academy of Science, Beijing 100190, People's Republic of China

Supporting Information

ABSTRACT: Gold nanodendrites with a long and densely branched morphology were fabricated by a seed-mediated method in a solution containing gold nanoparticles (AuNPs), bis(amidoethyl-carbamoylethyl)octadecylamine (C18N3), $HAuCl_4$, and the reducing agent ascorbic acid (AA). The length and density of the branches could be mediated by changing the AuNP seed and AA concentrations. The amphiphilic C18N3 molecules function as a template and induce the unique morphology of the AuNPs/C18N3 structures. The localized surface plasmon resonance (LSPR) peaks of the gold nanodendrites can be modulated from the visible (~530 nm) to the near-infrared region (~1100 nm) of the electromagnetic spectrum. Surface-enhanced Raman scattering (SERS) signals using rhodamine can also be mediated by changing the seed and AA concentrations. These unique highly branched gold nanodendrites with a narrow size distribution and tunable NIR and SERS spectra should have great potential in sensing applications.

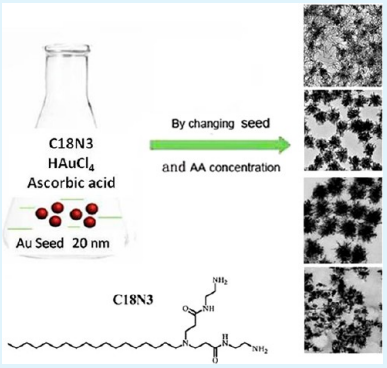

KEYWORDS: *NIR, SERS, gold nanodendrites, multiamine surfactant*

INTRODUCTION

Noble metal nanoparticles have attracted significant attention in recent years because of their fascinating properties and potential applications in catalysis, electronics, sensing, imaging, and biomedicine.[1−13] Among the many different noble metal nanomaterials, nanosized Au particles are especially attractive because they possess a unique size- and shape-dependent optical property known as localized surface plasmon resonance (LSPR).[14,15] Furthermore, gold nanostructures have shown excellent catalytic activity and can be used to fabricate surface-enhanced Raman scattering (SERS) substrates.[16−18] Various approaches have been used to synthesize gold nanostructures with a range of surface morphologies, including spheres, cubes, octahedrons, rods, plates, stars and flowers.[7,8,19−21] Among them, branched or star-shaped gold nanostructures consisting of a core body with protruding arms, sometimes referred to as nanoflowers or nanodendrites, have garnered particular interest because of their unique morphology and optical properties.[22−29] The core of the structure acts as an antenna, enhancing the electromagnetic field at the tips of the structure. In addition, the length and number of the dendrite branches has a strong effect on the LSPR signal.[30] It is therefore possible to tailor the frequency of the LSPR signal over a broad range by changing the core size and the morphology of the branches. To date, tremendous efforts have been devoted to the preparation of branched gold nanostructures.[21,31−34] However, it remains a challenge to control the morphology of the branches and to achieve broadly tunable plasmon resonances, especially in the near-IR region of the electromagnetic spectrum. In our group, we have successfully fabricated gold nano- and microplates as well as nanoflowers using bis(amidoethyl-carbamoylethyl)-octadecylamine (C18N3) amphiphilic molecules in aqueous solution under varying conditions.[35−37]

Herein, we present a facile method for the synthesis of gold nanodendrites with a long and highly dense branch morphology using a seed-mediated method in aqueous solution at room temperature, as shown in Scheme 1. $HAuCl_4$ was reduced by ascorbic acid (AA) in aqueous solution in the presence of spherical citrate-coated gold nanoparticles and C18N3 amphiphilic molecules. The LSPR peaks of the resultant gold nanodendrites can be modulated from the visible (~530 nm) to the near-infrared region (~1100 nm) of the spectrum by varying the length and the density of branches, which can be controlled by varying the amount of seeds and AA. We propose that C18N3 amphiphilic molecules function as a template and induce the unique morphology of the gold dendrite nanostructures.[36,38]

EXPERIMENTAL SECTION

Materials. Chloroauric acid ($HAuCl_4 \cdot H_2O$), sodium citrate, and ascorbic acid were obtained from the Beijing chemical plant. Ultrapure deionized water (Milli-Q MΩ cm^{-1}) was used for the preparation of all solutions. Bis(amidoethyl-carbamoylethyl)octadecylamine (C18N3)

Received: November 26, 2012
Accepted: July 2, 2013
Published: July 2, 2013

Scheme 1. Schematic Illustration of the Method for Preparing a Variety of Gold Nanodendrites

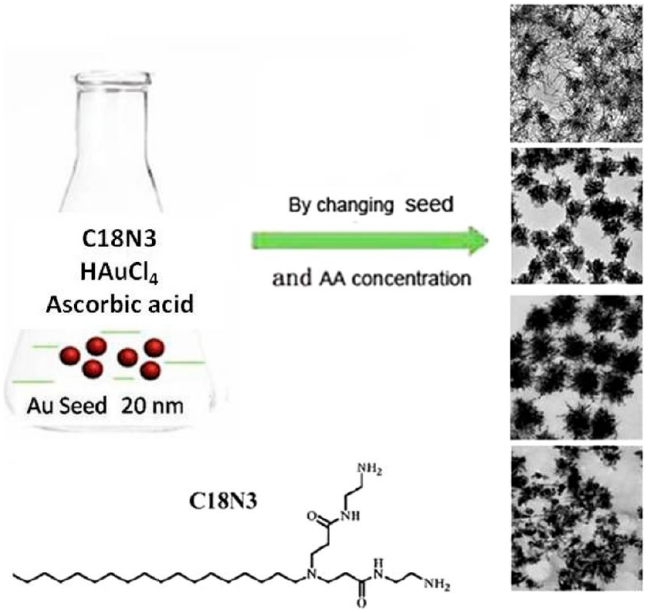

was synthesized using a two-step procedure as reported previously. Rhodamine 6G (R6G) was purchased from Aldrich.

Synthesis of Citrate-Coated Gold Seeds. Briefly, 0.15 mL of 2% (m/v) $HAuCl_4$ was added to 30 mL of ultrapure deionized water in a 50 mL flask. After the solution was brought to a boil while stirring, 0.375 mL of 2% (m/v) sodium citrate solution was added. The reaction was stopped after 30 min.[39] The characteristics of these gold seeds are shown in Supporting Information Figure 1S.

Synthesis of Gold Nanodendrites. In a typical procedure, 50 μL of citrate-coated gold seeds approximately 20 nm in diameter were added to 4 mL of growth solution consisting of C18N3 amphiphilic molecules (0.6 mM) and $HAuCl_4$ (0.25 mM). Subsequently, 10 μL of 0.1 M aqueous ascorbic acid (AA)[40] was added. After gentle shaking, the mixture was maintained at room temperature for 12 h. The suspension was centrifuged at 5000 rpm for 5 min, and the precipitates were collected and washed with distilled water several times before finally being redispersed in 1 mL of distilled water. The reactions were performed at room temperature (20–25 °C).

Characterization of Gold Nanostructures. The products were characterized by ultraviolet–visible (UV–vis) spectroscopy (Hitachi U-2800 spectrometer), scanning electron microscopy (SEM, Hitachi S4800, 10 kV), transmission electron microscopy (TEM JEOL-2010, 200 KV), and X-ray diffraction (XRD, Rigaku Dmax-2000, Ni-filter, Cu kα radiation). For the XRD measurements, the gold product was first dispersed in water, and several drops of the suspension were then placed on a clean glass slide and allowed to dry in the ambient air. For the TEM and SEM measurements, the suspension was either placed on a Formvar-coated copper grid or a silicon wafer, respectively, followed by air drying.

Raman Spectra Measurements. SERS measurements were performed using a confocal microprobe Raman spectrometer (Renishaw, inVia-Reflex). R6G was used as a probe molecule. First, R6G was dissolved in ethanol, producing a 1 mM solution. Gold nanodendrites prepared as described above were drop cast onto a silicon wafer and dried in ambient air. To ensure the formation of dense layers of gold nanodendrites, we drop cast several times after drying. Once the film was dry, a 3 μL 1 mM ethanol solution was added to the gold films. The SERS spectra were recorded using a 785 nm laser with an output power of 50 mW. The spectra were collected by focusing the laser onto the sample using a 50× objective, providing a spatial resolution of approximately 1 μm. The data acquisition time was 10 s for two accumulations. To test reproducibility, the measurements were performed at different positions on each sample.

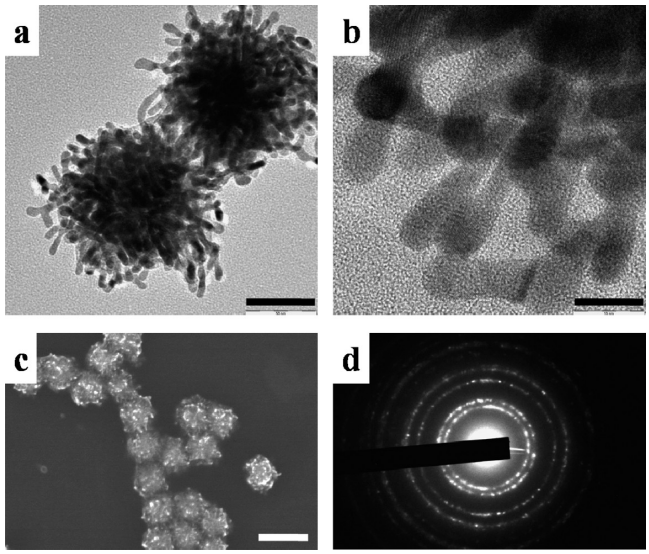

Figure 1. (a) TEM images of the gold nanodendrites. (b) TEM images of the gold nanodendrite branches at a higher magnification. (c) SEM images of the gold nanodendrites. (d) SAED pattern of the surface of a single gold nanodendrite. Scale bar: (a) 50, (b) 10, and (c) 200 nm.

RESULTS AND DISCUSSION

Figure 1a shows the transmission electron microscopy (TEM) images of the gold nanodendrites fabricated using the procedure detailed in the Experimental Section. The gold nanodendrites exhibit a branched morphology with an average size of approximately 100 nm, displaying a complex structure with a dense core and hierarchical branches. This type of reproducible structure for a nanodendrite complex has not been observed previously for gold nanomaterials. Figure 1b shows a TEM image of the branches at a higher magnification, clearly displaying the long and complex antenna-like branches. The average dimensions of the branches are a width of 4 nm and a length of 30 nm. The antenna-like branches are composed of a single crystal structure. Figure 1c shows a scanning electron microscopy (SEM) image that demonstrates the narrow size distribution of the gold nanodendrites and the surface roughness from the bright spot of the image. Figure 1d displays the selected-area electron diffraction (SAED) pattern of a single nanodendrite, suggesting that the nanodendrites are composed of many branches with random orientations.

The X-ray diffraction (XRD) patterns of the synthesized nanodendrites also reveal that the gold nanodendrites are a pure and well-crystallized Au crystal. Well-resolved peaks for the (111), (200), (220), and (311) diffraction planes of fcc Au are observed, as shown in Figure 2a. Both the X-ray diffraction (XRD) patterns and HRTEM image shown in Figure 2b reveal that all the branches were made from Au crystallites.

Figure 3 shows the SEM and TEM images of gold nanodendrites prepared using the standard procedure with a varying seed number. The images shown in Figure 3 indicate that the synthesized nanostructures possess a narrow size distribution and numerous surface branches. As the seed number increases, the gold nanodendrites show a similar morphology but are progressively smaller in size (Figures 3e, d, g, and h). When the highest concentration (1 mL) of seeds was added to the working solution, the complex was almost split into many small pieces.

dx.doi.org/10.1021/am401006b | ACS Appl. Mater. Interfaces 2013, 5, 6886–6892

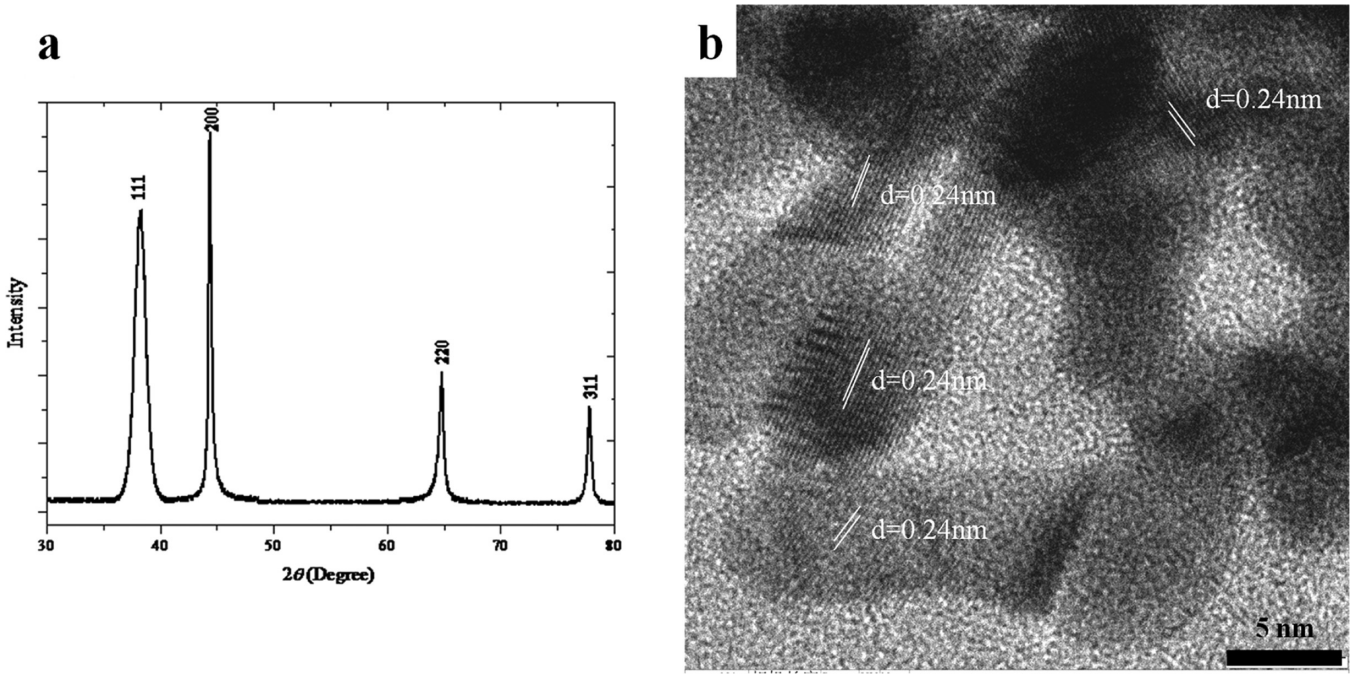

Figure 2. (a) XRD pattern of the gold nanodendrites. (b) HRTEM images of the gold nanodendrites. Scale bar: 5 nm.

Figure 4 shows that the length of the branches could be controlled by varying the reductant (AA) amount while keeping all other conditions constant. The SEM and TEM images of the gold nanodendrites were obtained by using 0.2 mL of gold seed, 0.6 mM C18N3, and varying volumes of AA. The [AA]/[$HAuCl_4$] ratios in the growth solutions in Figure 4 are 0.1:1, 0.5:1, 0.7:1, 1:1, and 1.4:1. In particular, when the [AA]/[$HAuCl_4$] ratio is 0.1:1, the reaction rate is very slow, and anisotropic growth is favored; therefore, the length of the arms of the branches increases. The long branches are single crystal structures with an average diameter of 4 nm, as shown in Supporting Information Figure S3b and S4b, and also possess some furcations to form flower-like 3D superstructures. In contrast, an increase in the reduction rate due to an increase in the AA concentration can promote the deposition of gold atoms on the seed surface and thus shorten the length of the branches. This phenomenon is consistent with the LaMer Model and the Weimarn rules for colloid particle formation in a solution,[41,42] which states that after seed formation of AuNPs, the crystallite growth rate is proportional to the total concentration of the precipitated substance. As shown in Figure 4, at high concentrations of AA, many new Au^0 atoms were quickly produced and deposited on the surfaces of the AuNP/C18N3 complexes, increasing the size of the dense core of the complex and decreasing the length of the branches of the resulting gold nanodendrites. Thus, AA concentration plays an important role in the modification of the morphology of gold nanodendrites.[43,44]

In the formation of the branch morphology, the multiamine surfactant C18N3 molecules play a crucial role. As reported by Matijevic, the pH, solvent, and specific chelating agent used during formation will change the morphology of the colloids.[45] The adsorption or chelating of C18N3 with the AuNPs will decrease the interface energy of the AuNPs seeds on the interface and favor the growth of the branches of gold nanodendrites.

The optical properties of the gold nanodendrites were further characterized by UV−vis−NIR spectroscopy. Precise control over the morphology of the gold nanodendrites can be

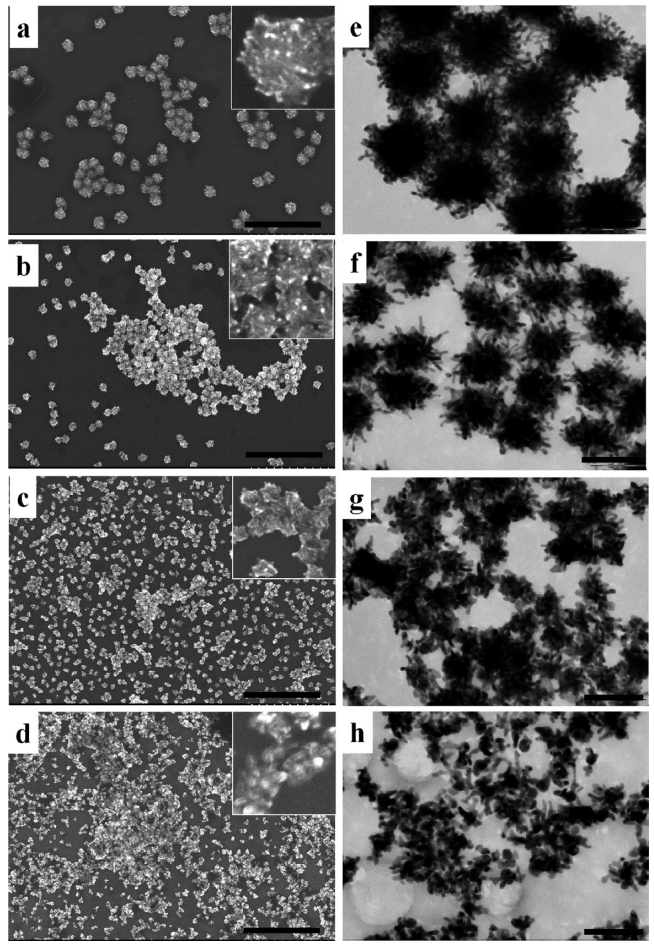

Figure 3. SEM (a, b, c, d) and TEM (e, f, g, h) images of gold nanostructures obtained under the same reaction conditions used in Figure 1 (the standard procedure), but with varying seed number: (a, e) 0.05, (b, f) 0.2, (c, g) 0.5, and (d, h) 1 mL. The scale bars of the SEM and TEM images are 1 μm and 100 nm, respectively.

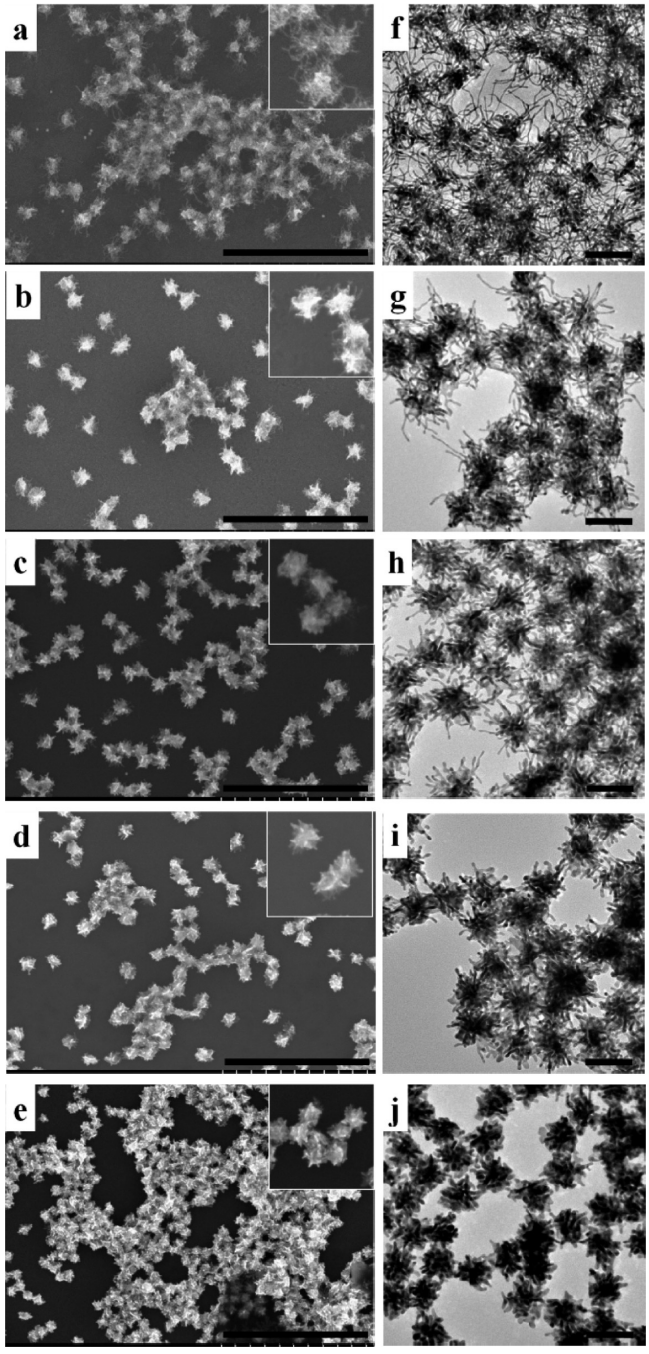

Figure 4. SEM and TEM images of gold nanostructures obtained using 0.2 mL of gold seed and 0.6 mM C18N3 with varying concentration of AA: (a, f) 2, (b, g) 5, (c, h) 7, (d, i) 10, and (e, j) 14 μL. Scale bar: (a, b, c, d, e) 1 μm and (f, j, h, i, j) 100 nm.

demonstrated by comparing their optical properties. Figure 5 shows the UV−vis−NIR spectra and corresponding images of the gold nanodendrites obtained using varying seed volumes, as described above. Similar to star and branch-shaped gold nanostructures,[24,46] the nanodendrites displayed two distinct LSPR peaks that can be assigned to the dipolar resonances localized around either the branches or the central core. An increasing red-shift of the LSPR peaks occurs as a function of increasing branch length. Significantly, the peak position of the main longitudinal resonance mode corresponding to the tip-localized plasmon could be red-shifted to wavelengths of over

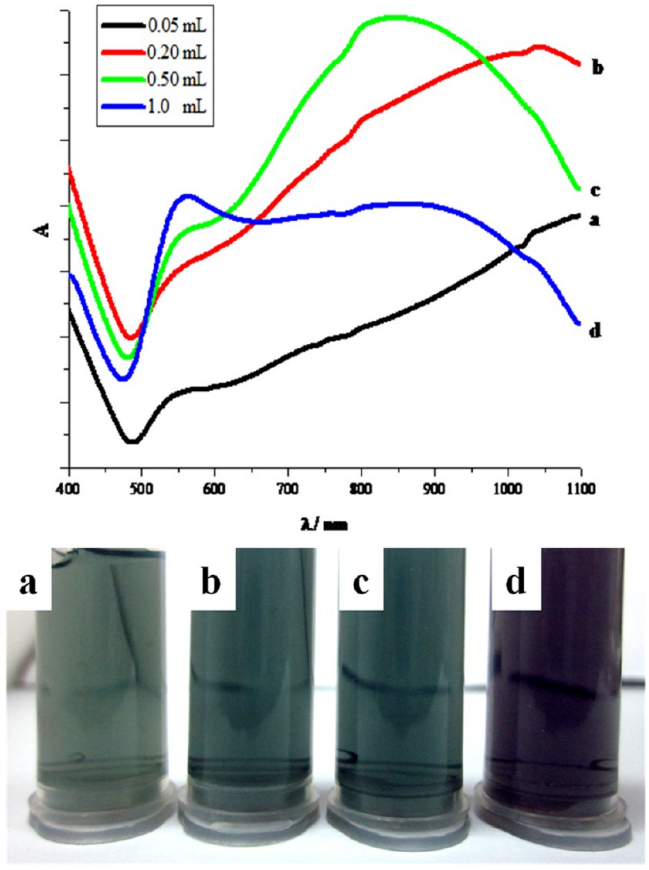

Figure 5. UV−vis−NIR absorption spectra and photographs taken from gold nanodendrites obtained using different volumes of seeds.

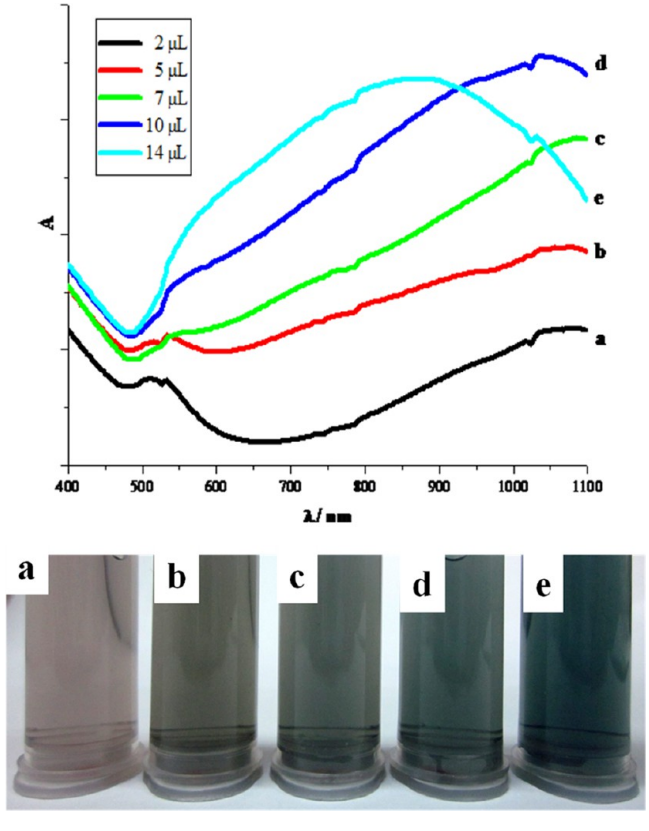

Figure 6. UV−vis-NIR absorption spectra and photograph taken of gold nanodendrites prepared using varying volumes of AA.

dx.doi.org/10.1021/am401006b | ACS Appl. Mater. Interfaces 2013, 5, 6886−6892

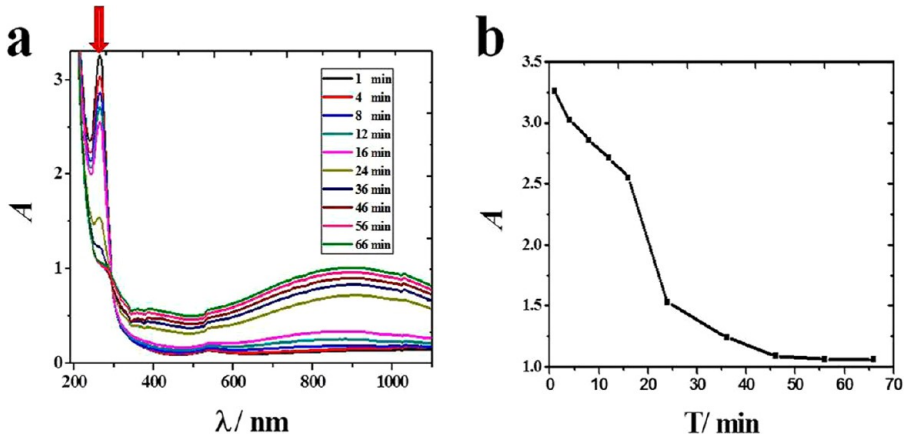

Figure 7. Kinetic analysis of the gold nanodendrite fabrication process using UV−vis spectroscopy: (a) time-resolved UV−vis spectra of the reaction solutions containing 0.6 mM C18N3, 0.2 mL seeds, and 10 μL AA. (b) Kinetic analysis of the peak intensity of Au^{+} (262 nm).

Scheme 2. Schematic Illustration of the Influence of AA and Au Seed Concentration on the Formation and Morphology of Gold Nanodendrites

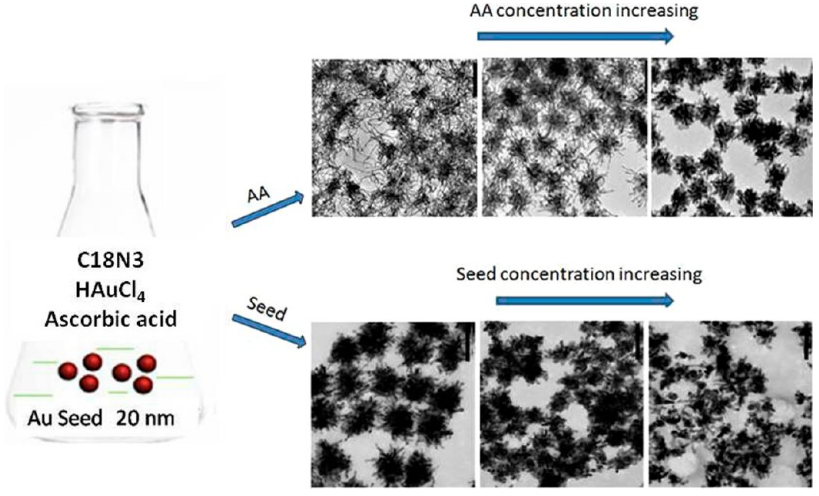

1100 nm by decreasing the volume of seed to 0.05 mL. This level of tunability in the NIR has not been achieved with nanostars.[21,26,30,47,48] Interestingly, when the volume of seed was 1 mL, the peak at 530 nm was more intense than the longitudinal resonance mode at 830 nm. These results are consistent with the morphological changes observed by SEM and TEM imaging (Figure 3), implying that the core size did not change and the surfaces of the cores were partially encapsulated by branches. Although the peak position of the longitudinal LSPR band shifted in response to morphology changes, the position of the LSPR band corresponding to the core only marginally shift, to approximately 530 nm, reflecting a nearly constant core size.

Varying the volume of AA resulted in a similar trend in the LSPR peak positions, as shown in Figure 6. The peak position of the longitudinal resonance mode red-shifted from 850 to 1100 nm as the volume of AA decreased from 14 to 2 μL. This optical behavior can be clearly observed with the naked eye, as shown in the photograph in Figure 6. By correlating the LSPR spectra with the SEM and TEM images of the gold nanodendrites shown in Figure 4, the red shift can be attributed to the lengthening of the nanodendrite branches as the volume of AA decreases. Notably, an LSPR peak similar to that observed in gold nanorods appeared when the volume of AA used was 2 μL. These results demonstrate that our synthetic method allows us to obtain highly controlled gold nanodendrites with various morphologies, providing an efficient way to finely tune their optical properties.

The fabrication process was kinetically analyzed using UV−vis spectroscopy, as shown in Figure 7. On the basis of the kinetic analysis of the Au^{+} peak intensity (262 nm), we propose that the gold atoms were initially deposited on the surface of the gold seeds/C18N3 complex at a slow reduction rate, which was followed by rapid branch growth. Here, we used a new strategy by adding 20 nm AuNp as a seed for the growth of crystallites before the reduction begins. The C18N3 surfactant plays an important role as the shape directing agent, pH adjusting agent, and the chelating agent in the formation of the gold nanodendrites.

Nanoflowers or nanostars were recently exploited as powerful SERS substrates exhibiting strong SERS enhancement factors.[23,49−52] Figure 8 shows the SERS spectra of R6G molecules on gold nanodendrites. The main vibrational features of the R6G molecules are apparent, as shown in Supporting Information

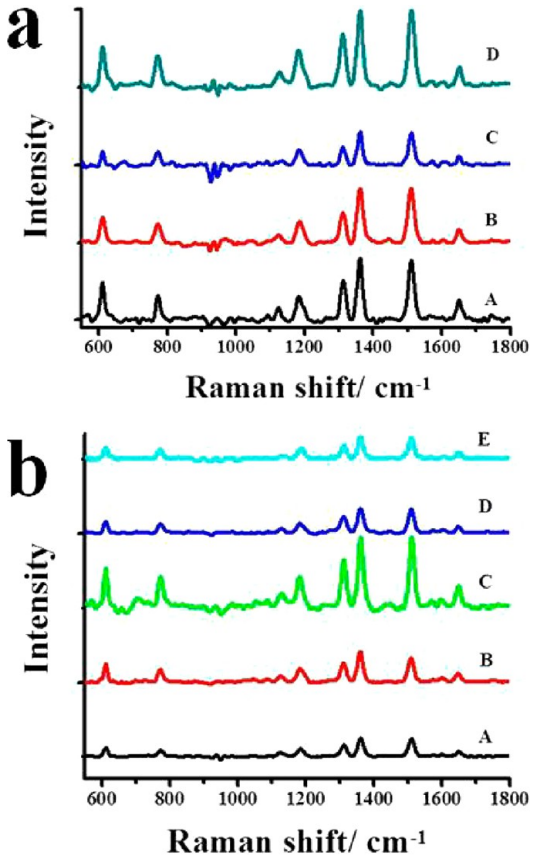

Figure 8. SERS signals obtained from R6G molecules on gold nanodendrites. (a) Gold nanodendrites obtained using varying volumes of seed: A, 0.05 mL; B, 0.2 mL; C, 0.5 mL; D, 1 mL. (b) Gold nanodendrites obtained using varying volumes of AA: A, 2 μL; B, 5 μL; C, 7 μL; D, 10 μL; E, 14 μL.

Figure S5. The SERS spectra shows that gold nanostructures with a higher density of surface branches exhibited stronger SERS enhancing signals than nanostructures with a lower density of surface branches. We speculate that the enhancement effect on the SERS signal can be attributed to the long and densely packed branches on the surface of the gold nanodendrites, and further investigations are underway.

CONCLUSION

In summary, we have demonstrated a facile method for the synthesis of gold nanodendrites with a long and densely packed branch morphology based on seeded growth. The success of this controlled growth method can be attributed to the mild reaction conditions, including the seeding of the reaction, a weak reducing agent, and a multiamine surfactant. The LSPR peaks of the resulting gold nanodendrites can be modulated from the visible (~530 nm) to the near-infrared region (~1100 nm) of the spectra by tailoring the length and density of the branches using varying amounts of seed and AA. The fabricated gold nanostructures exhibited variable UV–vis absorption and SERS enhancement as a function of branch morphology, indicating their potential in biolabeling, imaging, biosensing, and therapeutic applications, as well as a variety of sensing applications. Although this strategy has great advantages for the preparation of different types of gold nanodendrites, the exact mechanism is not yet clear, and further investigation is necessary.

ASSOCIATED CONTENT

Supporting Information

TEM images, UV–vis spectroscopy, and the SERS spectra of R6G solid powder. This information is available free of charge via the Internet at http://pubs.acs.org/.

AUTHOR INFORMATION

Corresponding Author

*E-mail: jiangl@iccas.ac.cn.

Notes

The authors declare no competing financial interest.

ACKNOWLEDGMENTS

This research is supported by the National Natural Science Foundation of China (Grant Nos. 20933007, 91127012, 21161130521, 21021003).

REFERENCES

(1) Zhou, Z.-Y.; Tian, N.; Li, J.-T.; Broadwell, I.; Sun, S.-G. *Chem. Soc. Rev.* **2011**, *40* (7), 4167–4185.
(2) Xie, W.; Qiu, P.; Mao, C. *J. Mater. Chem.* **2011**, *21* (14), 5190–5202.
(3) Rycenga, M.; Cobley, C. M.; Zeng, J.; Li, W.; Moran, C. H.; Zhang, Q.; Qin, D.; Xia, Y. *Chem. Rev.* **2011**, *111* (6), 3669–3712.
(4) Morton, S. M.; Silverstein, D. W. *Chem. Rev.* **2011**, *111* (6), 3962–3994.
(5) Mayer, K. M.; Hafner, J. H. *Chem. Rev.* **2011**, *111* (6), 3828–3857.
(6) Hartland, G. V. *Chem. Rev.* **2011**, *111* (6), 3858–3887.
(7) Guo, S.; Wang, E. *Nano Today* **2011**, *6* (3), 240–264.
(8) Chen, H. M.; Liu, R.-S. *J. Phys. Chem. C* **2011**, *115* (9), 3513–3527.
(9) De, M.; Ghosh, P. S.; Rotello, V. M. *Adv. Mater.* **2008**, *20*, 1–17.
(10) Chen, J.; Lim, B.; Lee, E. P.; Xia, Y. *Nano Today* **2009**, *4* (1), 81–95.
(11) Cobley, C.; Skrabalak, S.; Campbell, D.; Xia, Y. *Plasmonics* **2009**, *4* (2), 171–179.
(12) Henzie, J.; Lee, J.; Lee, M. H.; Hasan, W.; Odom, T. W. *Annu. Rev. Phys. Chem.* **2009**, *60* (1), 147–165.
(13) Wang, L.; Imura, M.; Yamauchi, Y. *ACS Appl. Mater. Interfaces* **2012**, *4* (6), 2865–2869.
(14) Eustis, S.; El-Sayed, M. A. *Chem. Soc. Rev.* **2006**, *35* (3), 209–217.
(15) Myroshnychenko, V.; Rodriguez-Fernandez, J.; Pastoriza-Santos, I.; Funston, A. M.; Novo, C.; Mulvaney, P.; Liz-Marzan, L. M.; Garcia de Abajo, F. J. *Chem. Soc. Rev.* **2008**, *37* (9), 1792–1805.
(16) Han, X.; Wang, D.; Huang, J.; Liu, D.; You, T. *J. Colloid Interface Sci.* **2011**, *354* (2), 577–584.
(17) Zhu, Z.; Meng, H.; Liu, W.; Liu, X.; Gong, J.; Qiu, X. *Angew. Chem., Int. Ed.* **2011**, *50* (7), 1593–1596.
(18) Tong, L.; Zhu, T.; Liu, Z. *Chem. Soc. Rev.* **2011**, *40* (3), 1296–1304.
(19) Niu, W.; Xu, G. *Nano Today* **2011**, *6* (3), 265–285.
(20) Lee, G.; Cho, Y.-S.; Park, S.; Yi, G.-R. *Korean J. Chem. Eng.* **2011**, *28* (8), 1641–1650.
(21) Guerrero-Martínez, A.; Barbosa, S.; Pastoriza-Santos, I.; Liz-Marzán, L. M. *Curr. Opin. Colloid Interface Sci.* **2011**, *16* (2), 118–127.
(22) Lee, Y.; Park, T. G. *Langmuir* **2011**, *27* (6), 2965–2971.
(23) Maiorano, G.; Rizzello, L.; Malvindi, M. A.; Shankar, S. S.; Martiradonna, L.; Falqui, A.; Cingolani, R.; Pompa, P. P. *Nanoscale* **2011**, *3* (5), 2227–2232.
(24) Pallavicini, P.; Chirico, G.; Collini, M.; Dacarro, G.; Dona, A.; D'Alfonso, L.; Falqui, A.; Diaz-Fernandez, Y.; Freddi, S.; Garofalo, B.; Genovese, A.; Sironi, L.; Taglietti, A. *Chem. Commun.* **2011**, *47* (4), 1315–1317.

(25) Ren, Y.; Xu, C.; Wu, M.; Niu, M.; Fang, Y. *Colloids Surf., A* **2011**, *380* (1−3), 222−228.
(26) Rodriguez-Lorenzo, L.; Romo-Herrera, J. M.; Perez-Juste, J. *J. Mater. Chem.* **2011**, *21* (31), 11544−11549.
(27) Sahoo, G. P.; Bar, H.; Bhui, D. K.; Sarkar, P.; Samanta, S.; Pyne, S.; Ash, S.; Misra, A. *Colloids Surf., A* **2011**, *375* (1−3), 30−34.
(28) Trigari, S.; Rindi, A.; Margheri, G.; Sottini, S.; Dellepiane, G.; Giorgetti, E. *J. Mater. Chem.* **2011**, *21* (18), 6531−6540.
(29) Van de Broek, B.; Frederix, F.; Bonroy, K.; Jans, H.; Jans, K.; Borghs, G.; Maes, G. *Nanotechnology* **2011**, *22*, 015601.
(30) Barbosa, S.; Agrawal, A.; Rodríguez-Lorenzo, L.; Pastoriza-Santos, I.; Alvarez-Puebla, R. n. A.; Kornowski, A.; Weller, H.; Liz-Marzán, L. M. *Langmuir* **2010**, *26* (18), 14943−14950.
(31) Sau, T. K.; Rogach, A. L. *Adv. Mater.* **2010**, *22* (16), 1781−1804.
(32) Wang, L.; Liu, C.-H.; Nemoto, Y.; Fukata, N.; Wu, K. C. W. *RSC Adv.* **2012**, *2* (11), 4608−4611.
(33) Wang, L.; Imura, M.; Yamauchi, Y. *Cryst. Eng. Commun.* **2012**, *14* (22), 7594−7599.
(34) Lim, B.; Xia, Y. *Angew. Chem., Int. Ed.* **2011**, *50* (1), 76−85.
(35) Wang, W.; Lu, W.; Jiang, L. *J. Phys. Chem. B* **2008**, *112* (5), 1409−1413.
(36) Lin, G. H.; Lu, W. S.; Cui, W. J.; Jiang, L. *Cryst. Growth Des.* **2010**, *10* (3), 1118−1123.
(37) Jia, W.; Li, J.; Lin, G.; Jiang, L. *Cryst. Growth Des.* **2011**, *11* (9), 3822−3827.
(38) Xiao, J.; Qi, L. *Nanoscale* **2011**, *3* (4), 1383−1396.
(39) Frens, G. *Nature* **1973**, *241* (105), 20−22.
(40) Gou, L.; Murphy, C. *Chem. Mater.* **2005**, *17* (14), 3668−3673.
(41) Lamer, V. K.; Barnes, M. D. *J. Colloid Interface Sci.* **1946**, *1* (71), 79.
(42) Barlow, D. A.; Baird, J. K.; Su, C.-H. *J. Cryst. Growth* **2004**, *264* (1−3), 417−423.
(43) Wang, L.; Hu, C.; Nemoto, Y.; Tateyama, Y.; Yamauchi, Y. *Cryst. Growth Des.* **2010**, *10* (8), 3454−3460.
(44) Sau, T. K.; Murphy, C. J. *J. Am. Chem. Soc.* **2004**, *126* (28), 8648−8649.
(45) Matijevic., E. *Chem. Mater.* **1993**, *5* (4), 412−426.
(46) Kuo, C.-H.; Huang, M. H. *Langmuir* **2005**, *21* (5), 2012−2016.
(47) Senapati, D.; Singh, A. K.; Khan, S. A.; Senapati, T.; Ray, P. C. *Chem. Phys. Lett.* **2011**, *504* (1−3), 46−51.
(48) Moukarzel, W.; Fitremann, J.; Marty, J.-D. *Nanoscale* **2011**, *3* (8), 3285−3290.
(49) Khoury, C. G.; Vo-Dinh, T. *J. Phys. Chem. C* **2008**, *112* (48), 18849−18859.
(50) Jeong, G. H.; Lee, Y. W.; Kim, M.; Han, S. W. *J. Colloid Interface Sci.* **2009**, *329* (1), 97−102.
(51) Nalbant Esenturk, E.; Hight Walker, A. R. *J. Raman Spectrosc.* **2009**, *40* (1), 86−91.
(52) Joseph, D.; Geckeler, K. E. *Langmuir* **2009**, *25* (22), 13224−13231.